Inorganic Chemistry

Article

pubs.acs.org/IC

A Family of $Co^{II}Co^{III}_3$ Single-Ion Magnets with Zero-Field Slow Magnetic Relaxation: Fine Tuning of Energy Barrier by Remote Substituent and Counter Cation

Yuan-Yuan Zhu,*[,†,‡] Yi-Quan Zhang,[‡,§] Ting-Ting Yin,[†] Chen Gao,[‡] Bing-Wu Wang,[‡] and Song Gao*[,‡]

[†]School of Chemistry and Chemical Engineering, Hefei University of Technology and Anhui Key Laboratory of Advanced Functional Materials and Devices, Hefei 230009, China

[‡]Beijing National Laboratory for Molecular Sciences, State Key Laboratory of Rare Earth Materials Chemistry and Applications, College of Chemistry and Molecular Engineering, Peking University, Beijing 100871, China

[§]Jiangsu Key Laboratory for NSLSCS, School of Physical Science and Technology, Nanjing Normal University, Nanjing 210023, China

Supporting Information

ABSTRACT: The synthesis, structures, and magnetic properties of a family of air-stable star-shaped $Co^{II}Co^{III}_3$ complexes were investigated. These complexes contain only one paramagnetic Co(II) ion with the approximate D_3 coordination environment in the center and three diamagnetic Co(III) ions in the peripheral. Magnetic studies show their slow magnetic relaxation in the absence of an applied dc field, which is characteristic behavior of single-molecule magnets (SMMs), caused by the individual Co(II) ion with approximate D_3 symmetry in the center. Most importantly, it was demonstrated that the anisotropy energy barrier can be finely tuned by the periphery substituent of the ligand and the countercation. The anisotropy energy barrier can be increased significantly from 38 K to 147 K.

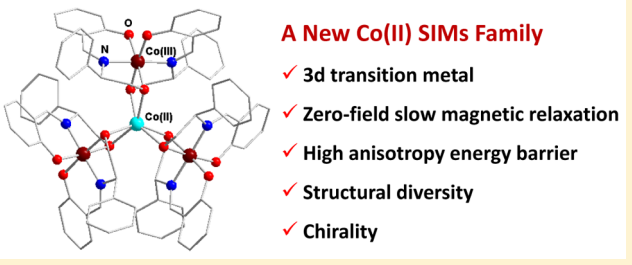

INTRODUCTION

Single-molecule magnets (SMMs) are individual molecules that exhibit slow magnetic relaxation at low temperature.[1] Since the first SMM ($Mn_{12}OAc$) was discovered in the 1990s,[2] much insightful research has been performed on this type of magnetic entity, because of its potential applications in information storage, quantum computing, and spin operation.[3,4] Among the oceans of multinuclear transition-metal complexes, only a few of the exchange-coupled clusters can reach relatively high relaxation energy barriers (U_{eff}), high blocking temperatures (T_B), and bistability at zero magnetic field, which are key properties of an SMM.[1,5] In most cases, high blocking temperature and bistability at zero magnetic field are even more difficult to obtain than high relaxation barriers. In 2003, slow magnetic relaxation stemming from a single paramagnetic center was observed in the compound $Tb(III)Pc_2$ by Ishikawa et al.[6] The slow magnetic relaxation barrier can reach as high as 331 K. Because of the mononuclear characteristics, this type of SMM is also known as a single-ion magnet (SIM). This interesting result has prompted new research interest toward developing mononuclear metal complexes as SMMs. Thereafter, several lanthanide- and actinide-based SIMs have been synthesized.[7] For lanthanide and actinide ions, the spin−orbit coupling is great enough to compensate for any quenching effect from the ligand field, so that they are suitable mononuclear paramagnetic centers for constructing SIMs. A question then naturally emerges: Is it possible to find an SIM showing slow magnetic relaxation coming from a single transition metal ion, like the single 4f or 5f type SIMs mentioned above? The spin−orbit coupling in 3d transition-metal ions, however, is usually much weaker than the ligand field, so that the first-order orbital angular momentum is largely quenched, which makes the observation of slow magnetic relaxation from a mononuclear 3d transition-metal ion is more difficult than that of 4f or 5f analogues. However, recent studies have revealed that mononuclear transition-metal complexes can also possess SMMs behavior through rational structural design. More than 10 years ago, Gao et al. found examples of slow magnetic relaxation under a nonzero dc field from some coordination polymers containing magnetically isolated Fe(III), Cu(II), and Mn(II) ions; however, these works lack of understanding of the relaxation mechanism.[8] Over the last five years, the study on transition-metal-based SIMs has developed very quickly. By using the design strategy of low coordination number, weak ligand field, and special coordination environment, several examples of slow relaxation behavior in the absence of dc field or under an applied dc field from mononuclear transition-metal ions such as Co(II),[9,10] Fe(I),[11] Fe(II),[12] Fe(III),[13] Ni(I),[14] Mn(III),[15] and Re(IV)[16] have been

Received: March 6, 2015
Published: May 18, 2015

DOI: 10.1021/acs.inorgchem.5b00526
Inorg. Chem. 2015, 54, 5475−5486

reported. However, the examples of transition-metal-based SIMs displaying slow relaxation in the absence of dc field are still limited. Until now, only very limited examples of zero-field slow relaxation stemming from a single 3d transition-metal ion have been reported. They are $(Ph_4P)^+_2[Co^{II}(XPh)_4]^{2-}$ (X = O, S, Se),[10a,b] $(Ph_4P)_2[Co^{II}(C_3S_5)_2]$,[10e] (PNP)$Fe^{III}Cl_2$ (where PNP = *N*[2-P(CHMe$_2$)$_2$-4-methylphenyl]$_2^-$),[13] $[Fe^I(C(SiMe_3)_3)_2]^-$,[11] $[Co(P(S)\{[N(CH_3)N{=}CHC_3N_2H_3]_3)\}][(NO_3)_2]$,[10d] and $(HNEt_3)^+(Co^{II}Co^{III}{}_3L^3{}_6)^-$.[10c]

In 2013, we reported an air-stable star-shaped $Co^{II}Co^{III}{}_3$ cluster (**1**) with only one paramagnetic Co(II) ion in an approximate D_3 coordination environment.[10c] This interesting compound displays slow magnetic relaxation behavior in the absence of dc field and possesses anisotropy energy barrier as high as 109 K. It represents the first example of SMM behavior in a mononuclear six oxygen-coordinate Co(II) complex. Based on the chiral characteristic, this enantiopure complex is also a type of multifunctional molecular material that possesses both magnetic and optical properties. As a continuation of our previous work, we designed and synthesized a series of $Co^{II}Co^{III}{}_3$ analogues by modifying the Schiff base ligands with different substituents and changing the counter cations. Deep magnetic research demonstrated that the anisotropy energy barrier (U_{eff}) can be finely tuned in a wide range by the structural modification. For some complexes, the effective anisotropy energy barriers are even higher than that of **1**. Herein, we report the synthesis, characterization, and magnetism, especially the interesting fine-tuning of the relaxation barriers of these $Co^{II}Co^{III}{}_3$ family compounds.

EXPERIMENTAL SECTION

Reagents and General Procedures. All starting materials were commercially available at analytical grade and used without further purification. All reactions were carried out under aerobic condition. The synthesis procedure of the Schiff base ligands was described in our previous paper.[10c,21]

Caution! *Although not encountered in our experiments, perchlorate salts in the presence of organic ligands are potentially explosive. Only a small amount of the materials should be prepared and handled with care.*

*Synthesis of $[H(NEt_3)]^+[Co^{II}Co^{III}{}_3(L^1{}_R)_6]^-$) (**2R**).* A solution of $H_2L^1{}_R$ (181 mg, 0.75 mmol), HCOONa·2H$_2$O (104 mg, 1 mmol) and Et$_3$N (0.225 mL, 1.5 mmol) in methanol (30.0 mL) was stirred at room temperature until all the reactants was dissolved, and a solution of $Co(ClO_4)_2$·6H$_2$O (183 mg, 0.5 mmol) in methanol (10.0 mL) was then added dropwise to the bright yellow solution. Some precipitated brown solid was formed but disappeared when the solution was stirred under atmosphere for ∼10 min. The color of the solution was turned to dark brown. The solution was filtrated and left to stand at room temperature with slow evaporation. Dark red granular single crystals of **2R** were obtained after several days. Yield: 60%−70%.

Althoughthe $HOOC^-$ anion is not a component of the complex, HCOONa is very important to promote the growth of high-quality crystals in this experiment.

2R. Anal. Calcd for $C_{96}H_{94}Co_4N_7O_{12}$·3H$_2$O·2MeOH: C, 62.22; H, 5.75; N, 5.18. Found: C, 62.02; H, 6.00; N, 5.24. IR (single crystal): ν = 3643(w), 3058(w), 3025(w), 2972(w), 2921(w), 2857(w), 2667(w), 1637(s), 1599(m), 1536(m), 1493(w), 1467(m), 1455(s), 1441(m), 1383(w), 1348(m), 1319(m), 1252(w), 1199(m), 1148(m), 1126(m), 1065(m), 1030(m), 966(w), 947(m), 899(m), 833(w), 796(w), 754(m), 736(w), 705(m), 651(w), 628(w), 615(w). HRMS (ESI-MS): Calcd for $C_{90}H_{80}Co_4N_6O_{12}^+$: 1672.31567, Found: 1672.31408; Calcd for $C_{96}H_{95}Co_4N_7O_{12}^+$: 1773.43612, Found: 1773.43539; Calcd for $C_{102}H_{110}Co_4N_8O_{12}^+$: 1874.55657, Found: 1874.55032 (cation mode). Calcd for $C_{90}H_{78}Co_4N_6O_{12}^-$: 1670.30112, Found: 1670.29716 (anion mode).

*Synthesis of $[H(NEt_3)]^+[Co^{II}Co^{III}{}_3(L^1{}_S)_6]^-$) (**2S**).* The enantiomer complex of **2S** was synthesized by using $H_2L^1{}_S$ as a ligand in the same way to that of **2R**. Anal. Calcd for $C_{96}H_{94}Co_4N_7O_{12}$·3H$_2$O·2MeOH: C, 62.22; H, 5.75; N, 5.18. Found: C, 62.53; H, 5.75; N, 5.50. IR (single crystal): ν = 3642(w), 3058(w), 3025(w), 2972(w), 2921(w), 2857(w), 2667(w), 1636(s), 1599(m), 1536(m), 1493(w), 1467(m), 1455(s), 1441(m), 1383(w), 1348(m), 1319(m), 1252(w), 1198(m), 1148(m), 1125(m), 1065(m), 1030(m), 966(w), 947(m), 899(m), 833(w), 796(w), 754(m), 736(w), 705(m), 651(w), 628(w), 615(w). HRMS (ESI-MS): Calcd for $C_{90}H_{80}Co_4N_6O_{12}^+$: 1672.31567, Found: 1672.31062; Calcd for $C_{96}H_{95}Co_4N_7O_{12}^+$: 1773.43612, Found: 1773.43217; Calcd for $C_{102}H_{110}Co_4N_8O_{12}^+$: 1874.55657, Found: 1874.54579 (cation mode). Calcd for $C_{90}H_{78}Co_4N_6O_{12}^-$: 1670.30112, Found: 1670.29826 (anion mode).

*Synthesis of $[H(DBU)]^+[Co^{II}Co^{III}{}_3(L^1{}_R)_6]^-$ (**3R**).* A mixture of $H_2L^1{}_R$ (362 mg, 1.5 mmol) and DBU (1,8-diazabicyclo[5.4.0]undec-7-ene) (0.45 mL, 3 mmol) in methanol (20.0 mL) was stirred at room temperature. A dark brown precipitate was generated as soon as the solution of $Co(ClO_4)_2$·6H$_2$O (366 mg, 1 mmol) in methanol (10.0 mL) was added dropwise, and the mixture was stirred at room temperature for 12 h. The resulting solution was filtered by reduced pressure. The dark brown precipitate was dried under vacuum and then redissolved in hot DMF (40.0 mL). Dark red crystals with thin plate were obtained within 2 weeks in 60%−70% yield by slow evaporation of the resulting solution. Anal. Calcd for $C_{99}H_{95}Co_4N_8O_{12}$·3DMF·$^1/_4H_2$O: C, 63.33, H, 5.73, N, 7.52. Found: C, 62.92, H, 5.99, N, 7.13. IR (single crystal): ν = 3641(w), 3055(w), 3024(w), 2920(w), 2854(w), 1674(m), 1635(s), 1597(m), 1535(m), 1493(w), 1466(m), 1454(s), 1385(w), 1346(m), 1319(m), 1254(w), 1200(w), 1149(w), 1126(w), 1092(w), 1065(w), 1030(m), 949(w), 899(w), 833(w), 795(w), 756(m), 737(w), 706(w), 652(w). HRMS (ESI-MS): Calcd for $C_{90}H_{78}Co_4N_6O_{12}^-$: 1670.30112, Found: 1670.29727 (anion mode).

*Synthesis of $[H(NEt_3)]^+[Co^{II}Co^{III}{}_3(L^2{}_R)_6]^-$ (**4R**).* A mixture of $H_2L^2{}_R$ (446 mg, 1.5 mmol) and Et$_3$N (4.3 mL, 3 mmol) in methanol (20.0 mL) was stirred at room temperature. A dark brown precipitate was generated as soon as the solution of $Co(ClO_4)_2$·6H$_2$O (366 mg, 1 mmol) in methanol (10.0 mL) was added dropwisely, and the mixture was stirred at room temperature for 12 h. The resulting solution was filtered by reduced pressure. The dark brown precipitate was dried under vacuum and then redissolved in hot DMF (40.0 mL). Dark red crystals with thin plate were obtained within 2 weeks in 60%−70% yield by slow evaporation of the resulting solution. Anal. Calcd for $C_{120}H_{142}Co_4N_7O_{12}$·3H$_2$O: C, 66.60; H, 6.89; N, 4.53. Found: C, 66.56; H, 6.75; N, 4.51. IR (single crystal): ν = 3649(w), 3061(w), 3026(w), 2959(m), 2904(m), 2864(m), 2708(w), 1953(w), 1895(w), 1817(w), 1759(w), 1637(s), 1611(m), 1529(m), 1478(s), 1422(w), 1379(m), 1362(m), 1319(m), 1271(m), 1254(m), 1210(w), 1178(m), 1146(m), 1111(w), 1065(w), 1030(m), 964(w), 948(w), 919(w), 880(w), 845(m), 826(m), 805(w), 763(m), 747(w), 702(m), 654(w), 625(w). HRMS (ESI-MS): Calcd for $C_{114}H_{128}Co_4N_6O_{12}^+$: 2008.69128, Found: 2008.67820 (cation mode); Calcd for $C_{120}H_{143}Co_4N_7O_{12}^+$: 2109.81173, Found: 2109.79198 (cation mode).

*Synthesis of $[H(DBU)]^+[Co^{II}Co^{III}{}_3(L^3{}_R)_6]^-$ (**5R**).* Compound **5R** was synthesized by using $H_2L^3{}_R$ as the ligand in the similar way to that of **3R**. Anal. Calcd for $C_{99}H_{89}Br_6Co_4N_8O_{12}$·6DMF: C, 51.35, H, 4.83, N, 7.17. Found: C, 50.98, H, 4.67, N, 7.36. IR (single crystal): ν = 3645(w), 3059(w), 3028(w), 2920(w), 2858(w), 1666(w), 1639(s), 1589(m), 1520(w), 1493(w), 1462(s), 1419(m), 1373(m), 1315(m), 1265(w), 1246(w), 1196(w), 1173(m), 1134(w), 1065(w), 1030(m), 945(w), 872(w), 822(m), 764(w), 706(w), 690(w), 652(m), 602(w). HRMS (ESI-MS): Calcd for $C_{90}H_{72}Br_6Co_4N_6O_{12}^-$: 2143.76420, Found: 2143.76066 (anion mode).

*Synthesis of $[H(DIPEA)]^+[Co^{II}Co^{III}{}_3(L^4{}_R)_6]^-$ (**6R**).* A mixture of $H_2L^4{}_R$ (429 mg, 1.5 mmol) and DIPEA (*N*,*N*-diisopropylethylamine) (0.52 mL, 3 mmol) in methanol (20.0 mL) was stirred at room temperature. A dark brown precipitate was generated as soon as the solution of $Co(ClO_4)_2$·6H$_2$O (366 mg, 1 mmol) in methanol (10.0 mL) was added dropwise, and the mixture was stirred at room temperature for 12 h. The resulting solution was filtered by reduced pressure. The dark

DOI: 10.1021/acs.inorgchem.5b00526
Inorg. Chem. 2015, 54, 5475−5486

brown precipitate was dried under vacuum and then redissolved in hot DMF (40.0 mL). Dark red crystals with thin plate were obtained within 2 weeks in 60%−70% yield by slow evaporation of the resulting solution. Anal. Calcd for $C_{98}H_{92}Co_4N_{13}O_{24}$·4DMF: C, 55.89, H, 5.12, N, 10.07. Found: 55.48, H, 5.33, N, 10.46. IR (single crystal): ν = 3630(w), 3059(w), 3028(w), 2924(w), 2858(w), 1666(m), 1643(m), 1601(s), 1551(m), 1493(m), 1477(m), 1443(w), 1381(w), 1311(s), 1250(w), 1192(w), 1134(w), 1103(m), 1065(w), 1030(w), 949(w), 849(w), 829(w), 802(w), 756(w), 729(w), 698(w), 656(w), 602(w). HRMS (ESI-MS): Calcd for $C_{90}H_{72}Co_4N_{12}O_{24}^-$: 1940.21159, Found: 1940.20943 (anion mode).

Synthesis of $[H(DBU)]^+[Co^{II}Co^{III}_3(L^4_R)_6]^-$ ***(7R).*** This compound was synthesized by using $H_2L^4_R$ as the ligand in a manner similar to that used for **3R**. Anal. Calcd for $C_{99}H_{89}Co_4N_{14}O_{24}$·4.5DMF: C, 55.75, H, 5.01, N, 10.69. Found: 55.32, H, 5.35, N, 11.07. IR (single crystal): ν = 3290(w), 3147(w), 3059(w), 2928(w), 2858(w), 1662(w), 1647(w), 1601(m), 1551(w), 1493(w), 1473(m), 1443(w), 1381(w), 1358(w), 1311(s), 1250(w), 1203(w), 1099(m), 1030(w), 949(w), 845(w), 829(w), 760(w), 733(w), 698(w), 656(w), 621(w), 602(w). HRMS (ESI-MS): Calcd for $C_{90}H_{72}Co_4N_{12}O_{24}^-$: 1940.21159, Found: 1940.20976 (anion mode).

Synthesis of $(n\text{-}Bu_4N)^+[Co^{II}Co^{III}_3(L^4_R)_6]^-$ ***(8R).*** A mixture of TBAB (tetra-*n*-butyl ammonium bromide) (967 mg, 3 mmol) and KOH (168 mg, 3 mmol) in methanol (20.0 mL) was stirred at room temperature for 10 min, then $H_2L^4_R$ (429 mg, 1.5 mmol) was added. A dark brown precipitate was generated as soon as the solution of $Co(ClO_4)_2$·$6H_2O$ (366 mg, 1 mmol) in methanol (10.0 mL) was added dropwise, and the mixture was stirred at room temperature for 12 h. The resulting solution was filtered by reduced pressure. The dark brown precipitate was dried under vacuum and then redissolved in hot DMF (40.0 mL). Dark red crystals with thin plate were obtained within 2 weeks in 60%−70% yield by slow evaporation of the resulting solution. Anal. Calcd for $C_{106}H_{108}Co_4N_{13}O_{24}$·3DMF: C, 57.48, H, 5.41, N, 9.33. Found: C, 57.07, H, 5.68, N, 9.82. IR (single crystal): ν = 3059(w), 3028(w), 2962(w), 2924(w), 2858(w), 1670(w), 1643(w), 1601(m), 1551(m), 1493(m), 1477(m), 1443(w), 1381(w), 1311(s), 1250(w), 1192(w), 1134(w), 1099(w), 1068(w), 1030(w), 949(w), 849(w), 829(w), 756(w), 733(w), 698(w), 656(w), 602(w). HRMS (ESI-MS): Calcd for $C_{90}H_{72}Co_4N_{12}O_{24}^-$: 1940.21159, Found: 1940.20905 (anion mode).

Crystal Structure Determination. Crystals suitable for X-ray diffraction (XRD) were covered in a thin layer of polyisobutylene oil, mounted on a glass fiber attached to a copper pin or on a microloop, and placed under an N_2 cold stream.

The X-ray measurements of **2R**, **2S**, **5R**, and **8R** were carried on a Saturn724+ CCD diffractometer with a confocal monochromator using Mo Kα radiation (λ = 0.71073 Å) at 173 K. Intensities were collected using CrystalClear (Rigaku, Inc., 2008) technique and absorption effects were collected using the multiscan technique. The X-ray measurement of **3R** was carried on a Saturn724+ CCD diffractometer with a graphite monochromator using Mo Kα radiation (λ = 0.71073 Å) at 173 K. Intensities were collected using the CrystalClear (Rigaku, Inc., 2008) technique and absorption effects were collected using the multiscan technique. The X-ray measurement of **4R** was carried on a Nonius Kappa CCD diffractometer with Mo Kα radiation (λ = 0.71073 Å) at 200 K. The X-ray measurements of **6R** and **7R** were carried on Biological Macromolecules Station (1W2B beamline), Beijing Synchrotron Radiation Facility (BSRF), Institute of High Energy Physics, Chinese Academy of Sciences. The wavelength of synchrotron light source (λ) is 0.7 Å and the measured temperature is 100 K. Intensities were collected using the HKL2000 program and absorption effects were collected using the multiscan technique. Empirical absorption corrections were applied using the Sortav program. All structures were solved using SHELXS-97 program[17] and refined by a full matrix least-squares technique based on F^2 using the SHELXL 97 program.[18]

The calculated densities (ρ_{calcd}) observed by the X-ray analysis are 1.154 g cm^{-3} for **2R**, 1.161 g cm^{-3} for **2S**, and 0.930 g cm^{-3} for **7R**, which demonstrate that the densities of these crystals are lower than that of the normal crystal. Calculations using the CALC VOID option in PLATON[19] showed a potential solvent access area of 2654.4 Å^3 (26.0%) for **2R**, 2546.4 Å^3 (25.1%) for **2S**, and 5868.7 Å^3 (39.3%) for **7R** per unit cell of the complex. In the structure refinement, the disordered solvent molecules could not be modeled and were treated by SQUEEZE, in PLATON. Some solvent molecules and cations (water and methanol in **2R**/**S**, DMF and $[H(DBU)]^+$ in **7R**) might occupy in the void space, which were not included in the formula.

Magnetic Properties Measurements. Magnetic susceptibility data were collected using Quantum Design MPMS-XL SQUID and PPMS-9T (EC-II) magnetometers. All samples were performed on polycrystalline samples restrained in a frozen eicosane matrix or parafilm. dc susceptibility measurements of $\chi_M T$ curve were collected in the temperature range of 2−300 K under a dc field of 1 kOe. ac susceptibility measurements were obtained in a variety of temperature ranges under an ac field of 3 Oe, oscillating at frequencies of 100−10000 Hz, in the absence of a dc field or under a dc field of 1500 Oe. The magnetic susceptibility data were corrected for the diamagnetism of the samples using Pascal constants[20] and of the sample holder and parafilm by correction measurement.

RESULTS AND DISCUSSION

Synthesis of the $Co^{II}Co^{III}_3$ compounds. In this work, four types of chiral salicylaldehyde Schiff base ligands with different substituents in the *para*-position of the salicylaldehyde ring were used to synthesis the series of mixed valence $Co^{II}Co^{III}_3$ clusters. Our previous work showed that this type of chiral ligands could successfully be employed to construct star-shaped Fe^{III}_4 single-molecule magnets[21] and cubane-type $Cu^{II}_4O_4$ clusters.[22] During the synthesis procedure, four different counter cations ($H(NEt_3)^+$, $H(DIPEA)^+$, $H(DBU)^+$, and $(n\text{-}Bu)_4N^+$) were introduced into the complexes by using different bases (TEA, DIPEA, DBU, and TBAOH) as reaction precursor. The structures of Schiff base ligands and counter cations are illustrated in Scheme 1.

Scheme 1. Structures of Schiff Base Ligands and Counter Cations Used in This Work

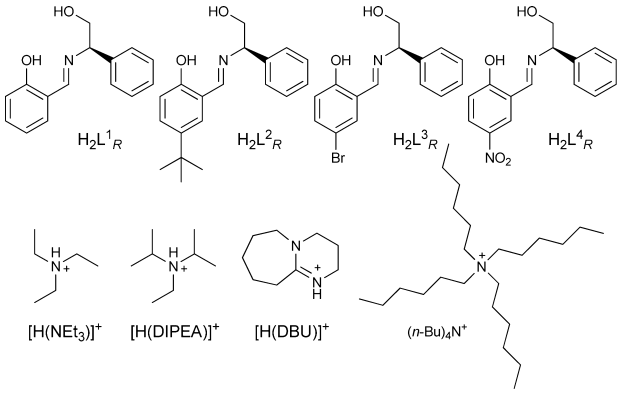

Theoretically, four ligands and four counter cations can form a maximum of 16 compounds in this family, if the chirality of ligand is disregarded. In this work, seven representative new compounds besides compound **1** were synthesized and studied in detail (see Table 1). Compounds **2**−**8** were obtained by the reaction of $Co(ClO_4)_2$·$6H_2O$, H_2L, and base in methanol (see Experimental Section for detail). The crystals of **2R** and **2S** were obtained from reaction solution directly and the others were recrystallized from hot DMF solution. The structures of eight complexes (**2R**/**S** and **3R**−**8R**) were all characterized by single crystal X-ray diffraction analysis.

DOI: 10.1021/acs.inorgchem.5b00526
Inorg. Chem. 2015, 54, 5475−5486

Table 1. Summary of the Substituents in Ligands and the Counter Cations in This Family of Compounds

compound	ligand	substituent	counter cation
1R	$H_2L^3{}_R$	Br	$[H(NEt_3)]^+$
2R	$H_2L^1{}_R$	H	$[H(NEt_3)]^+$
3R	$H_2L^1{}_R$	H	$[H(DBU)]^+$
4R	$H_2L^2{}_R$	*t*-Bu	$[H(NEt_3)]^+$
5R	$H_2L^3{}_R$	Br	$[H(DBU)]^+$
6R	$H_2L^4{}_R$	NO_2	$[H(DIPEA)]^+$
7R	$H_2L^4{}_R$	NO_2	$[H(DBU)]^+$
8R	$H_2L^4{}_R$	NO_2	$(n\text{-}Bu)_4N^+$

Structure Description. Similar to the reported compound **1**, the other family compounds (**2**−**8**) are all air-stable and have the general formula $A^+(Co^{II}Co^{III}{}_3L_6)^-$ (where A represents the counter cation; see Table 1 for detail). The single-crystal XRD analysis reveals that **2R** and **2S** are enantiomers and crystallized in the cubic space group $P2_13$. Compounds **3R**, **5R**, **6R**, and **8R** all crystallize in the orthorhombic space group $P2_12_12_1$. **4R** and **7R**, however, crystallize in the monoclinic space group $P2_1$ and the tetragonal space group $P4_32_12$, respectively (see Table 2). This series of compounds possess a similar skeleton (see Figure 1). The detailed data of bond lengths and angles for eight compounds are listed in Tables S1−S8. Three peripheral Co(III) ions form an equilateral triangle with one Co(II) ion in the center. The diamagnetic peripheral Co(III) ions are located in a slightly distorted octahedral coordination environment. However, the central Co(II) ion has a completely different coordination symmetry, which is a slightly distorted trigonal prism and approaches to D_3 symmetry. Because of the influence of the remote substituents of Schiff base ligands and counter cations in the lattice, the coordination symmetry of the series of star-shaped complexes have minor differences. Only **2R**/**S** have a crystallographically imposed C_3 axis. The three peripheral Co(III) ions in other compounds are not absolutely identical, so other compounds merely have a pseudo-C_3 axis. In our previous work, the exact valence of four Co ions within compound **1** has been identified by several cross evidence. Similarly, compounds **2**−**8** possess the same $(Co^{II}Co^{III}{}_3)^-$ skeleton. The negative charge of the tetranuclear cluster is compensated by a cation nearby, such as protonated organic base (TEA, DIPEA, and DBU) and quaternary ammonium cation $(n\text{-}Bu)_4N^+$. The crystallized products of this series of compounds are obtained in methanol for **2** (R and S configurations) and in DMF for **3**−**8**, some solvent molecules are co-crystallized in the crystal lattice between the clusters in the lattice. The sole paramagnetic center of Co(II) ions are magnetically well-isolated from each other by three peripheral diamagnetic Co(III) ions and Schiff base ligand in internal, and different counter cations and uncoordinated solvent molecules in external. The shortest distance between the Co(II) ions of neighboring clusters is larger than 15 Å. It implies that the magnetic exchange interaction between paramagnetic Co(II) ions is very weak and can be neglected.

In the study of $Fe^{III}{}_4$ series of SMMs, Cornia et al. used angular parameters to compare the deviation of coordination sphere from ideal trigonal prism (D_{3h}) symmetry.[22] Similarly, the local symmetry of central Co(II) ions in this series of compounds also deviates from ideal D_{3h} symmetry, to different degrees, so the angular parameters α, β, θ, ϕ, and γ was introduced for benefit of comparison (see Figure 2). The values of α and β can be measured from the crystal structures directly. The values of θ and ϕ are calculated from the average interbond angles α and β by using eqs 1 and 2:

$$\cos\theta = \sqrt{\frac{1 + 2\cos\alpha}{3}} \tag{1}$$

$$\cos\left(\frac{\phi}{2}\right) = \sqrt{\frac{3(1 + \cos\beta)}{4(1 - \cos\alpha)}} \tag{2}$$

The angle θ describes the distortion by trigonal compression ($\theta > 54.74°$) or elongation ($\theta < 54.74°$). The angle ϕ indicates the distortion by trigonal rotation. For octahedron and trigonal prisms, the values of ϕ are 60° and 0°, respectively. The angle γ is the "pitch" of the propeller structure, defined as the dihedral angle between the $Co^{II}O_2Co^{III}$ and $Co^{II}Co^{III}{}_3$ planes. It can be calculated from the angles θ and ϕ, according to eq 3:

$$\cos\gamma = \frac{\sin\left(\frac{\phi}{2}\right)}{\left[\sin^2\left(\frac{\phi}{2}\right) + \cot^2\theta\right]^{1/2}} \tag{3}$$

In this series of compounds (**1**−**8**), θ varies within a relatively limited range (from 54.70° to 56.36°). They are all close to the standard value of the trigonal prism (54.74°), indicating small trigonal compression for **1**−**7** and small trigonal elongation for **8** (see Figure 3b). The degrees of deviation of the θ values reveal that **1**, **5**, **6**, **7**, and **8** are close to the standard trigonal prism but the distortion in **2**, **3**, and **4** are significant. The values of ϕ and γ, however, span a wide range (from 16.01° to 23.47° for ϕ and from 73.01° to 78.81° for ϕ). Through analysis, it is found that compound **1** possesses the smallest ϕ angle and the largest γ dihedral angle. By contrast, the largest ϕ angle and the smallest γ dihedral angle are found in **4** (see Figure 3a). Similar to the $Fe^{III}{}_4$ series SMMs reported by Sessoli and Cornia et al.,[23] a good linear correlation also exists between γ and ϕ in this $Co^{II}Co^{III}{}_3$ family of SIMs (see Figure 3a). Because the three angles θ, ϕ, and γ are related by eq 3 and the change of θ is small, the propeller pitch γ is mainly changed by varying ϕ. According to the structure analysis, it can be concluded that small γ pitch, large ϕ angle, and departure from angle θ from 54.74° will cause the distortion from D_{3h} symmetry of central Co(II) ions. The results show that the twists of **2**, **3**, and **4** are much larger than those of **1**, **5**, **6**, **7**, and **8**.

To evaluate the symmetry of seven atoms in central Co(II) coordination sphere (one central Co(II) ion and six oxygen atoms) as a whole, the continuous symmetry measures (CShM) method[24] was also used to analyze the degree of deviation from the standard trigonal prism. The deviation parameter (S) values of eight central Co(II) ions based on D_{3h} symmetry are obtained from the SHAPE 2.0 program, which was developed by Alvarez and co-workers.[25] A Bigger S value implies the larger deviation of central Co(II) from the specific symmetry. The results are listed in Table 2, which show the local symmetry of **2**, **3**, and **4** are lower than that of others based on D_{3h} symmetry. The result is consistent with that obtained from the geometry parameters θ, ϕ, and γ. Meanwhile, the S values of eight compounds based on O_h symmetry was also obtained (see Table 3), which show the deviation of central Co(II) ions from octahedron is very large.

Static Magnetic Properties. Investigation of the magnetic properties of **2**−**8** was first proceeded via the analysis of variable-temperature dc magnetic susceptibility data. It was

DOI: 10.1021/acs.inorgchem.5b00526
Inorg. Chem. 2015, 54, 5475−5486

Table 2. Crystal Data, Data Collection, Solution, and Refinement Information of Compounds 2−8

	2R	2S	3R	4R	5R	6R	7R	8R
formula	$C_{96}H_{94}Co_4N_7O_{12}$	$C_{96}H_{94}Co_4N_7O_{12}$	$C_{108}H_{105.5}Co_4N_{11}O_{15.25}$	$C_{120}H_{148}Co_4N_7O_{15}$	$C_{117}H_{131}Br_6Co_4N_{14}O_{18}$	$C_{110}H_{120}Co_4N_{17}O_{28}$	$C_{96}H_{86}Co_4N_{14}O_{26}$	$C_{115}H_{129}Co_4N_{16}O_{27}$
formula weight	1773.50	1773.50	2037.25	2164.17	2736.54	2363.95	2087.51	2403.06
crystal system	cubic	cubic	orthorhombic	monoclinic	orthorhombic	orthorhombic	tetragonal	orthorhombic
space group	$P2_13$	$P2_13$	$P2_12_12_1$	$P2_1$	$P2_12_12_1$	$P2_12_12_1$	$P4_32_12$	$P2_12_12_1$
a (Å)	21.693(4)	21.652(7)	14.6121(16)	16.0739(2)	12.780(3)	12.583(3)	18.076(3)	19.547(4)
b (Å)	21.693(4)	21.652(7)	25.397(3)	22.6331(3)	19.188(4)	19.120(4)	18.076(3)	19.704(4)
c (Å)	21.693(4)	21.652(7)	27.754(3)	17.3613(2)	47.313(10)	45.556(9)	45.656(9)	29.635(6)
α (deg)	90	90	90	90	90	90	90	90
β (deg)	90	90	90	111.3030(4)	90	90	90	90
γ (deg)	90	90	90	90	90	90	90	90
V (Å^3)	10208(3)	10151(5)	10300.0(19)	5884.51(13)	11602(4)	10960(4)	14917(4)	11414(4)
Z	4	4	4	2	4	4	4	4
T (K)	173(2)	173(2)	173(2)	200(2)	173(2)	100(2)	100(2)	173(2)
F(000)	3692	3692	4242	2290	5572	4924	4304	5020
D_C (g cm^{-3})	1.154	1.161	1.314	1.221	1.567	1.433	0.930	1.398
μ (mm^{-1})	0.695	0.699	0.701	0.616	2.700	0.680	0.491	0.653
λ (Å)	0.71073	0.71073	0.71073	0.71073	0.71073	0.70000	0.70000	0.71073
crystal size (mm^3)	0.35 × 0.30 × 0.27	0.49 × 0.47 × 0.45	0.32 × 0.25 × 0.25	0.23 × 0.14 × 0.03	0.41 × 0.12 × 0.11	0.05 × 0.01 × 0.01	0.03 × 0.02 × 0.02	0.48 × 0.48 × 0.46
T_{min} and T_{max}	0.5497, 1.0000	0.5190, 1.0000	0.6593, 1.0000	0.834, 0.967	0.4432, 1.0000	0.9668, 0.9932	0.9854, 0.9902	0.7068, 1.0000
θ_{min}, θ_{max} (deg)	1.33, 25.35	1.33, 25.34	1.09, 27.24	3.46, 25.04	0.86, 26.38	1.91, 30.49	1.78, 27.49	1.24, 27.48
no. total reflns	35665	13727	71487	68421	62813	34919	17126	76800
no. unique reflns, R_{int}	6246, 0.0691	5863, 0.0536	23135, 0.0615	20383, 0.0660	23436, 0.0763	34919, 0.0328	17126, 0.0420	26097, 0.0585
no. obs. [$I \geq 2\sigma(I)$]	5887	4767	21701	14339	19073	29500	15618	24614
no. params	361	360	1269	1328	1302	1446	806	1469
$R1$ [$I \geq 2\sigma(I)$]	0.0791	0.0847	0.0662	0.0437	0.0929	0.0528	0.0482	0.0529
$wR2$ (all data)	0.2024	0.2243	0.1858	0.0882	0.2515	0.1459	0.1490	0.1550
S	1.099	1.060	1.127	0.949	1.189	1.041	1.053	1.169
$\Delta\rho^a$ (e/ Å^3)	0.450, −0.541	0.525, −0.486	1.116, −0.516	0.394, −0.315	1.491, −1.192	0.901, −1.219	0.785, −0.305	0.898, −1.081
max and mean Δ/σ^b	0.001, 0.000	0.001, 0.000	0.001, 0.000	0.001, 0.000	0.002, 0.000	0.001, 0.000	0.001, 0.000	0.001, 0.000
Flack parameter	0.09(3)	0.0012(2)	0.042(13)	0.012(8)	0.051(13)	0.0068(2)	0.045(11)	0.005(9)
CCDC	846094	846095	1051818	881923	1051820	1051821	1051822	1051823

[a]Max and min residual density. [b]Max and mean shift/σ.

DOI: 10.1021/acs.inorgchem.5b00526
Inorg. Chem. 2015, 54, 5475−5486

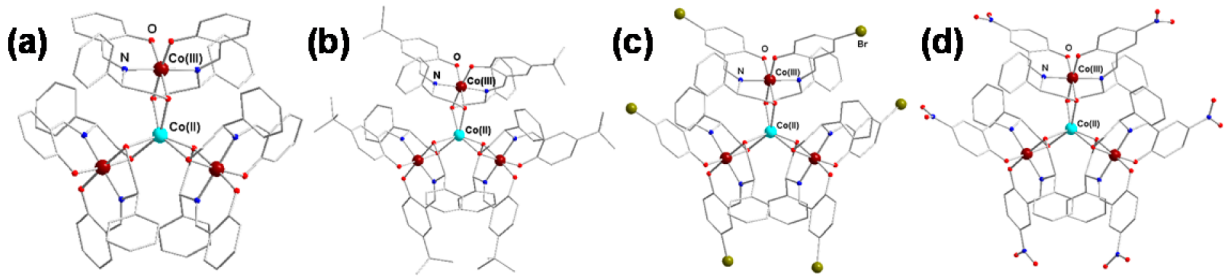

Figure 1. Single X-ray structures of complexes (a) **2**, (b) **4**, (c) **5**, and (d) **6**. Counter cations and hydrogen atoms have been omitted for clarity.

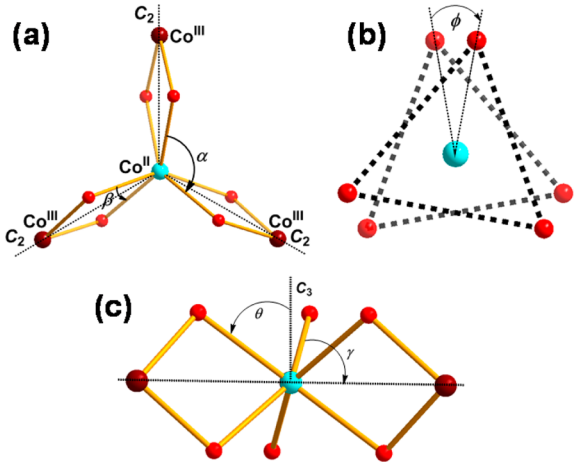

Figure 2. Definition of the angular parameters (a) α and β, (b) ϕ, and (c) γ and θ; all panels show the variables used in the structural analysis of the $Co^{II}Co^{III}_3$ propellers in this series, assuming ideal D_3 symmetry.

found that the temperature dependence of their molar magnetic susceptibilities are characteristic of noninteracting mononuclear Co(II) complexes. The $\chi_M T$ vs T plots of eight complexes are provided in Figure 4. At 300 K, the $\chi_M T$ values for **1**−**8** are 3.39, 3.24, 3.21, 3.19, 3.47, 3.11, 3.05, and 3.33 cm^3 K mol^{-1}, respectively. These values are significantly greater than the expected value of 1.875 cm^3 K mol^{-1} for an isotropic $S = {}^3/_2$ center with $g = 2.0$, which is due to the largely unquenched orbital momentum. Based on the $\chi_M T$ values at 300 K, the g values for **1**−**8** were calculated according to eq 4, giving the g values for **1**, **2**, **3**, **4**, **5**, **6**, 7, and **8** equal to 2.69, 2.63, 2.62, 2.61, 2.72, 2.58, 2.55, and 2.66, respectively.

$$\chi_M T = \frac{N\mu_B{}^2 g^2}{3k} S(S+1) \quad (4)$$

where

$$\frac{N\mu_B{}^2}{3k} = 0.125$$

Similar to other reported Co(II) SIMs, the $\chi_M T$ values at 300 K and g values are in the range of a single noninteracting d^7 Co(II) ion with a considerable contribution from the orbital angular momentum. The $\chi_M T$ curves remain roughly constant at the high-temperature range, then decrease slightly, ultimately reaching 2.73, 2.65, 2.38, 2.21, 2.45, 2.25, 2.32, and 2.91 at 2 K for **1**−**8**, respectively. The decrease of $\chi_M T$ values at low temperature range is mainly due to the depopulation of crystal field splitting levels. In order to get deep insight of the magnetic anisotropy for this series of compounds, the isothermal magnetization measurements of **2**, **3**, **4**, and **5** were measured up to a high dc field (8 or 12 T) at different temperatures (see Figures S1, S19, S28, and S38 in the Supporting Information). These results are similar to that of reported compound **1**. Because of the relative small total spin ($S = {}^3/_2$) of the whole molecule, the bifurcation of the M vs H/T plots appears to be significant at higher field range, implying the presence of high magnetic anisotropy.

Taken together, the results from the $\chi_M T$ and isothermal magnetization data indicate that this family of $Co^{II}Co^{III}_3$ complexes (**1**−**8**) all have highly anisotropic magnetic moments. The high magnetic anisotropy is attributed to the strong spin−orbital coupling of the central Co(II) ion.

Dynamic Magnetic Properties. Investigation of the slow magnetization relaxation is carried out via alternative current (ac) susceptibility measurements within the frequency range of

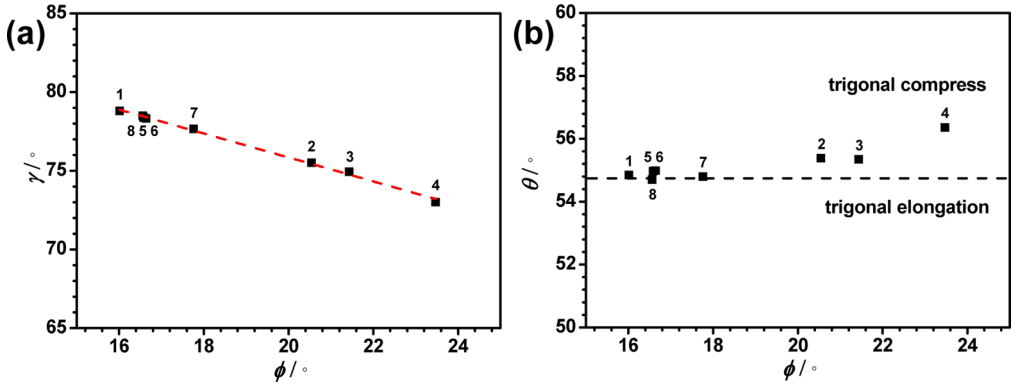

Figure 3. Correlation of three structural parameters in this series of $Co^{II}Co^{III}_3$ compounds **1**−**8**: (a) γ vs ϕ plot (red dash line indicates the best linear fitting) and (b) θ vs ϕ plot.

DOI: 10.1021/acs.inorgchem.5b00526
Inorg. Chem. 2015, 54, 5475−5486

Table 3. Selected Geometrical Parameters for Compounds 1−8[a]

						S	
No.	α	β	θ	ϕ	γ	D_{3h}	O_h
1R	90.164(0)	71.868(0)	54.85	16.01	78.81	2.221	9.548
2R	90.920(4)	71.839(4)	55.39	20.54	75.52	3.171	7.778
3R	90.864(8)	72.142(6)	55.35	21.43	74.94	3.353	7.489
4R	92.270(1)	70.803(1)	56.36	23.47	73.01	4.406	7.248
5R	90.333(14)	71.748(12)	54.97	16.58	78.38	2.341	9.284
6R	90.358(11)	71.725(11)	54.99	16.64	78.33	2.364	9.314
7R	90.092(12)	72.322(9)	54.80	17.76	77.66	2.454	8.775
8R	89.957(12)	72.260(11)	54.70	16.56	78.50	2.250	9.230

[a]Geometrical parameters have been averaged under the assumption of D_3 symmetry, and the numbers shown in parentheses are the associated standard deviations.

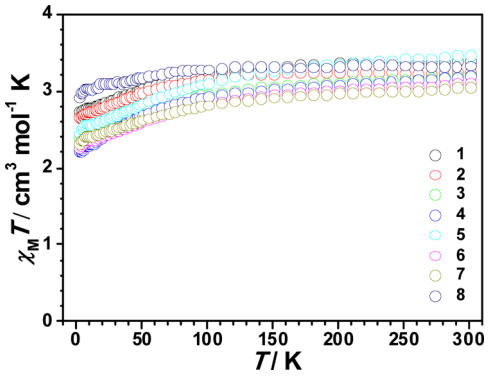

Figure 4. Temperature dependence of $\chi_M T$ under an applied dc field of 1 kOe at 2−300 K for polycrystalline samples of **1**−**8**.

100−10000 Hz. All compounds were found to display significant slow magnetic relaxation in the absence of dc field; both in-phase (χ') and out-of-phase (χ'') susceptibilities show significant frequency dependence at a broad temperature range (see Figure 5, as well as Figures S7, S22, S32, S41, S50, S59, and S68 in the Supporting Information). For **2** and **4** with protonated triethylamine as the countercation, the peaks from ν = 1000 Hz to ν = 10000 Hz appear in the range of 5−10 K and upturn strongly at low temperature, but broaden to shoulder at low frequencies. The upturn of χ'' at low frequencies and low-temperature range could be attributed to the impact of quantum tunneling of magnetization (QTM) on the thermal-assisted process, such as the situation in lanthanide-, actinide-, and other 3d-metal-based SIMs. The relaxation energy barriers (U_{eff}), fitted by Arrhenius law from the high-temperature regime of the relaxation, equal to 38 K and 43 K for **2** and **4**. Compound **3** is the analogue of **1** with the same Schiff base ligand $H_2L^1{}_R$, the difference is just to used protonated DBU to replace protonated triethylamine as countercation. However, the peak of χ'' appears at even higher temperature; the peaks from ν = 316 Hz to ν = 10000 Hz appear in the range of 6−13 K and the upturn at low temperature was slow, compared with that of **2**. It implies **3** possess a higher energy barrier, the fitted U_{eff} value is 52 K. Similar result is also found in the brominated series compounds. In previous work, we have reported the compound **1** ($L^2{}_R$ as ligand and protonated triethylamine as countercation) displays slow relaxation barrier as high as 109 K. Compound **5** was synthesized by using $[H(DBU)]^+$ to replace protonated triethylamine as countercation. Compared with **1**, compound **5** possesses even higher anisotropy energy barrier, with U_{eff} = 127 K. Since the $[H(DBU)]^+$ is a bulky cation group larger than $[H(Et_3N)]^+$, these results reveal that the bigger countercation may increase the anisotropy energy barrier in this series of compounds. The brominated compounds **1** and **5** possess a relaxation energy barrier larger than 100 K, which are much bigger than that of the archetype compound **2**, **3** and the *tert*-butyl substituted **4** that effective U_{eff} values are in the range of 30−50 K. Therefore, the substituent on the *p*-position may

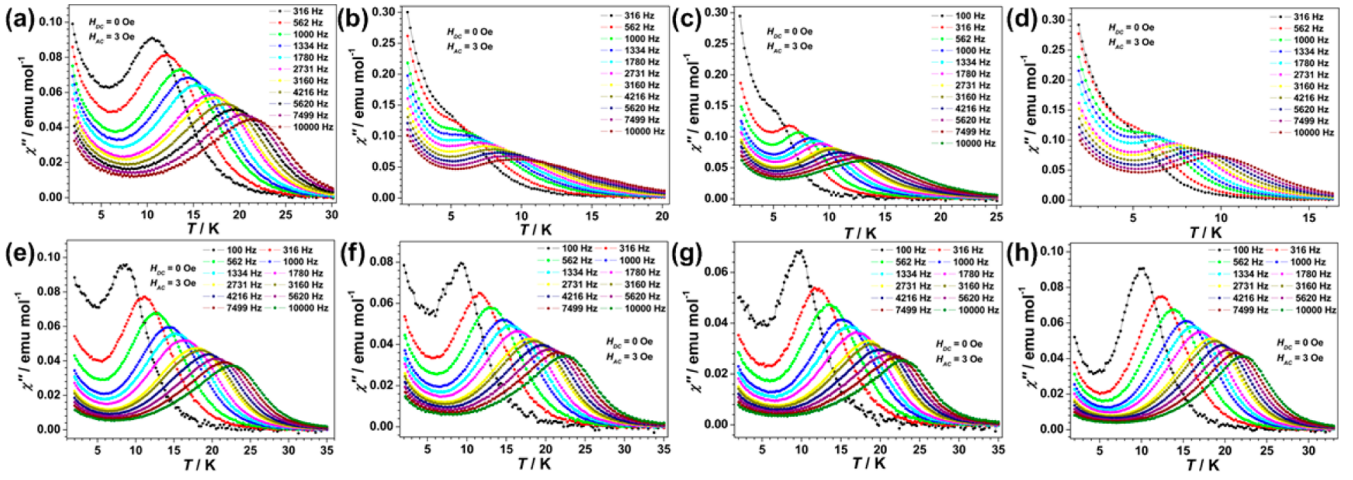

Figure 5. Temperature dependence of ac susceptibilities of (a) **1**, (b) **2**, (c) **3**, (d) **4**, (e) **5**, (f) **6**, (g) **7**, and (h) **8** at different frequencies in the absence of dc field.

DOI: 10.1021/acs.inorgchem.5b00526
Inorg. Chem. 2015, 54, 5475−5486

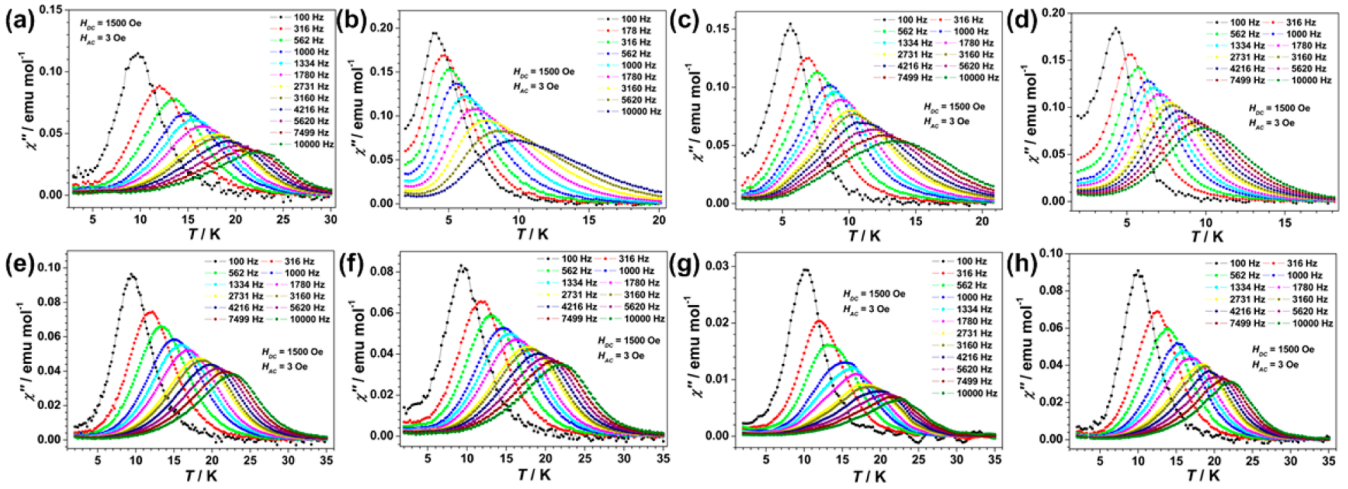

Figure 6. Temperature dependence of ac susceptibilities of (a) **1**, (b) **2**, (c) **3**, (d) **4**, (e) **5**, (f) **6**, (g) **7**, and (h) **8** at different frequencies under a dc field of 1500 Oe.

play an important role in influencing the relaxation energy barrier.

When the substituent in the *p*-position is a nitro group (NO_2), even-higher relaxation energy barriers are obtained. For series of compounds **6**, **7**, and **8** with $[H(DIPEA)]^+$, $[H(DBU)]^+$, and $[(n\text{-}Bu)_4N]^+$ as counter cations, the relaxation energy barriers (U_{eff}), which are fitted by the Arrhenius law, are equal to 129, 137, and 147 K, respectively.

For all compounds, the upturn of χ'' curve is observed at low temperature and low frequency range. The upturn of compounds **2**, **3**, and **4** is the most significant, impling the strong influence of quantum tunneling of the magnetization (QTM). The QTM phenomenon also exists in other compounds at low temperature and low frequency range. In order to reduce the QTM effect, ac measurements under a dc field of 1500 Oe were performed at various temperatures and frequencies, respectively (see Figure 6 and Figures S13, S25, S35, S44, S53, S62, and S71 in the Supporting Information). For all eight compounds, the dramatic disappearance of the upturns of χ'' indicated that QTM was almost effectively quenched at low temperature and low frequency range. Arrhenius analysis of the χ'' peaks under a dc field of 1500 Oe gives the U_{eff} values of eight complexes equal to 124, 41, 54, 45, 130, 134, 139, and 162 K, respectively. These values are all only slightly higher than those in the absence of dc field. The results reveal that QTM have strong influence to the relaxation process at low temperature range but less affects the slow relaxation process at high temperature range which determines the energy barrier.

In order to inspect the distribution of the relaxation time, the χ'' vs. χ' data of compounds **2**–**8** at different temperatures in the absence of dc field were all fitted by a modified Debye model[26] (see Figure 7 and Figures S15, S27, S37, S46, S55, and S64 in the Supporting Information). For compond **8**, the resulting α values vary in the range of 0.045–0.171 (the α value indicates deviation from the pure Debye model), which is within the range of superparamagnetism (see Table S15 in the Supporting Information). The α values increase to 0.171 at low temperatures and decrease toward zero at high temperatures. The Cole–Cole plots of other compounds give the similar results (see Tables S9–S14 in the Supporting Information). These results indicate the presence of an almost uniformly

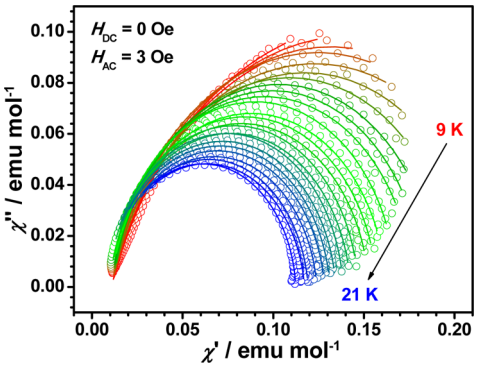

Figure 7. Cole–Cole diagram of **8R** in the absence of dc field from 9 K to 21 K (ac frequencies from 100 Hz to 10 000 Hz, 0.5 K interval).

distributed relaxation process in the range of the measured temperatures.

Theoretical Calculation and Magnetostructural Correlation Studies. To get deep insight of the magnetic anisotropy, the zero-field splitting parameters (D) and the energy separation between the two lowest KDs (Δ) of this family compounds were calculated using the CASSCF/RASSI method. In order to simplify the calculation, some approximation was employed. The three peripheral diamagnetic Co(III) ions were replaced by Zn(II) ions. In the detailed calculation, MOLCAS 7.8 program package[27] with complete active space second-order perturbation theory (CASPT2) was used to calculate the D and E values of the $(Co^{II}O_6(CH_3)_6Zn_3)$ fragment (see Figure 8) extracted from each compounds. To calculate the Co(II) fragment, the influence of the neighboring Co(III) ions have been simulated by the closed-shell Zn(II) *ab initio* embedding model potentials (AIMP; Zn.ECP.Lopez-Moraza.0s.0s.0e-AIMP-$KZnF_3$).[28] The only removed atoms are those connected to the Zn(II) AIMP from the outer side of the molecule.

The basis sets for all atoms were atomic natural orbital from the MOLCAS ANO-RCC library. The following contractions were used: [6s5p3d2f1g] for Co; [4s3p2d] for close O, [3s2p] for distant C, and [2s] for H. The spin–orbit coupling was handled separately in the restricted active space state interaction (RASSI-SO) procedure. The active electrons in 10

DOI: 10.1021/acs.inorgchem.5b00526
Inorg. Chem. 2015, 54, 5475–5486

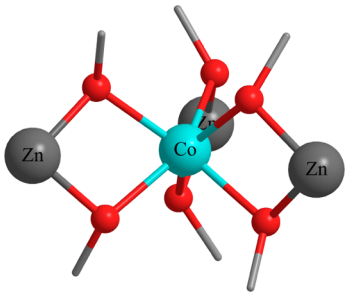

Figure 8. Calculated $Co^{II}O_6(CH_3)_6Zn^{II}_3$ fragment; H atoms have been omitted for clarity.

active spaces include all 7 3d electrons, and the mixed spin-free states are 50 (all from 10 quadruplets; all from 40 doublets).

According to calculation results, the magnetic easy axes were successfully obtained. In this family of compounds, the directions of easy axis are all approximately along the C_3-axis of the whole $Co^{II}Co^{III}_3$ cluster. For compound **2**, as an example, the calculated local easy magnetic axis of the ground KDs in Co(II) ion is shown in Figure 9. Other compounds possess the

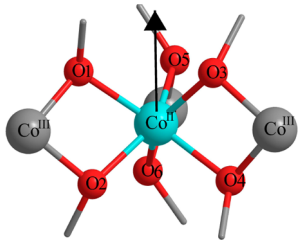

Figure 9. Scheme of the local main magnetic axis of the ground Kramers doublet (KD) of Co(II) ion in complex **2R**.

similar local easy magnetic axes. The calculated energy separation between the two lowest KDs (Δ), D, E and the effective g_{eff} values (x, y, z) for the lowest KDs using CASPT2, and the experimental U_{eff} values in the absence of dc field and a dc field of 1500 Oe of **1**−**8** are summarized in Table 4. These results show that, in this series of compounds, the energy barriers from the CASSCF-based calculation are much higher than the experimental values. In this family of compounds, the ground-state wave function is mainly composed of microstates with $M_J = \pm 9/2$ and $\pm 3/2$, and mixed with a small contribution of microstates with $M_J = \pm 7/2$ and $\pm 1/2$. The first excited-state wave function is mainly formed by microstates with $M_J = \pm 7/2$ and $\pm 1/2$, and mixed with a small component of microstates with $M_J = \pm 5/2$. The same components in the ground and first excited states increase the possibility of QTM and reduce the effective barrier of thermal activated magnetic relaxation. Similar to the rare-earth-based SIMs, the relatively small quantum number of angular momentum and no exchange coupling between the paramagnetic centers are two main reasons to cause the QTM process in 3d SIMs. The QTM effect was also verified in the magnetization hysteresis measurements (see Figures S2 and S29 in the Supporting Information). Although this series of compounds possess relative high relaxation energy, magnetization hysteresis, which is another important character of magnetic bistability of SMMs, was not observed, because of the strong QTM.

In Table 4, we only give the calculated D and E values of **2**−**4**, since the splitting of the two lowest KDs is much larger than the energy separation (Δ) between the lowest spin-free states for the other complexes (see Tables S16 and S17 in the Supporting Information). Thus, the energies in Table 3 cannot be understood as a zero-field splitting of a given $S = {}^3/_2$ level for complexes **1** and **5**−**8**. They have very strong spin−orbit coupling, and so that the spin−orbit coupled (J) ground states are split into several m_J states. Moreover, the energy separations between the two lowest KDs (Δ) for **2**−**4** are much smaller than those of other compounds, which are in accordance with the experimental U_{eff} values. As a comparison, the D and E values of complexes **2R**−**4R** were also obtained by fitting to the experimental $\chi_M T$ vs T plots using PHI program (see Table 4 and Figure S73 in the Supporting Information).[29] The results show the fitted D values of three complexes are close to the calculated results using CASPT2.

To explore the magnetostructural correlations for the eight complexes, we calculated the energy separation between the two lowest KDs (Δ) of the model structure **2R** with the variation of the structural parameters θ and ϕ (the other angles in Table 2 are dependent on θ and ϕ) using CASPT2.[30] The variation scope of θ and ϕ has covered the actual values of eight complexes. In the first calculations, the values of θ and ϕ were changed separately. The calculated Δ values are shown in Table 5, where the Δ values of the model structure **2R** decrease with the increase of ϕ, but increase with the increase of θ. However, the variations of Δ are much smaller, compared to those between the eight complexes (see Table 4).

To further investigate the influence of structural parameters, next we changed the values of θ and ϕ of the model structure **2R** simultaneously to correlate their Δ values. The calculated results are shown in Table 6; it was found the Δ values increase largely with the decrease of the values of θ and ϕ, especially

Table 4. Calculated Energy Barrier between the Two Lowest KDs Δ, D and E and the Effective g_{eff} Values (x, y, z) for the Lowest KDs Using CASPT2, and the Experimental U_{eff} Values in the Absence of a dc Field and under a dc Field of 1500 Oe for 1−8

	D (E) (cm^{-1}) calcu	D (|E|) (cm^{-1}) PHI	Δ (cm^{-1})	g_{eff}	U_{eff} (cm^{-1})	
					zero dc field	1500 Oe dc field
1R			305.7	0.015, 0.016, 9.793	76.2	86.7
2R	−34.4 (2.54)	−24.7 (0.05)	69.4	0.253, 0.276, 7.249	26.6	28.7
3R	−40.6 (2.13)	−35.2 (0.17)	81.6	0.237, 0.224, 7.466	36.4	37.8
4R	−28.8 (4.88)	−21.6 (0.03)	60.0	0.885, 1.096, 7.096	30.0	31.5
5R			306.5	0.012, 0.012, 9.822	88.8	90.9
6R			302.0	0.020, 0.020, 9.752	90.2	93.7
7R			294.3	0.008, 0.008, 9.656	95.8	97.2
8R			280.9	0.035, 0.035, 9.678	102.8	113.3

DOI: 10.1021/acs.inorgchem.5b00526
Inorg. Chem. 2015, 54, 5475−5486

Table 5. Calculated Energy Separation between the Two Lowest KDs Δ of the Model Structure 2R with the Variations of θ and ϕ Using CASPT2

θ (deg)	Δ (cm^{-1})	ϕ (deg)	Δ (cm^{-1})
53.4	58.3	12.5	82.3
54.4	62.6	16.5	75.7
55.4	69.4	20.5	69.4
56.4	79.7	24.5	49.2

when the value of θ approaches that of the standard trigonal prism (54.74°).

Table 6. Calculated Energy Separation Δ between the Two Lowest KDs of the Model Structure 2R with the θ and ϕ (deg) Changed Simultaneously Using CASPT2

θ, ϕ (deg)	Δ (cm^{-1})
54.4, 16.5	301.2
55.4, 20.5	69.4
56.4, 24.5	58.6

According to the calculation results in Tables 5 and 6, it can be concluded that changing the values of θ and ϕ separately has a small influence on the Δ value. The decrease of the values of θ and ϕ simultaneously will enhance the energy barrier significantly. For a standard trigonal prism (D_{3h} symmetry), the values of θ and ϕ are 54.74° and 0°, respectively. The calculation results demonstrate that the approach to the standard trigonal prism will cause a larger energy separation Δ.

Experimental and theoretical results all indicate that the magnetic anisotropy of this family of compounds stems from the central Co(II) ion. The local symmetry of central Co(II) ion strongly influences the anisotropy energy barrier. The *ab initio* calculation results demonstrate that the magnetic easy axis is along the pseudo-C_3 axis. The deviation from ideal D_{3h} symmetry can change the electron structure of Co(II) ion and cause the contribution of transverse zero-field splitting. It may influence the component of the ground-state and first excited-state wave function; therefore, tune the effective anisotropy energy barrier accordingly. The structural parameters can be used to correlate the calculated energy separation (Δ) and effective anisotropy energy barrier (U_{eff}). According to the analysis in Structural Description section, it is found that three angular parameters (θ, ϕ, and γ) and CShM calculation (S) can be used to describle the structural characteristic of central Co(II) ion quantitatively. Normally, deviation from ideal symmetry will introduce the contribution of transverse anisotropy. Small γ pitch, large ϕ angle, departure of θ angle from 54.74°, and large S value will cause the distortion of D_{3h} symmetry and *vice versa*. According to the structural analysis, it is found that the deviations of **2**, **3**, and **4** are much larger than that of others. Indeed, the anisotropy energy barriers (U_{eff}) of **2**, **3**, and **4** are also much lower than that of **1**, **5**, **6**, **7**, and **8**. Angular parameter γ is an effective parameter to describe the "pitch" of propeller structure in trigonal prism coordination symmetry. Figure 10 shows the relationship between the magnetic anisotropy (calculated energy barrier Δ and experimental value U_{eff}) and the angular parameter γ. The small γ pitch and large magnetic anisotropy are found in **1**, **5**, **6**, **7**, and **8**, and the large γ pitch and small magnetic anisotropy are found in **2**, **3**, and **4**. These results show that the approach to D_{3h} symmetry is important to obtain a high anisotropy

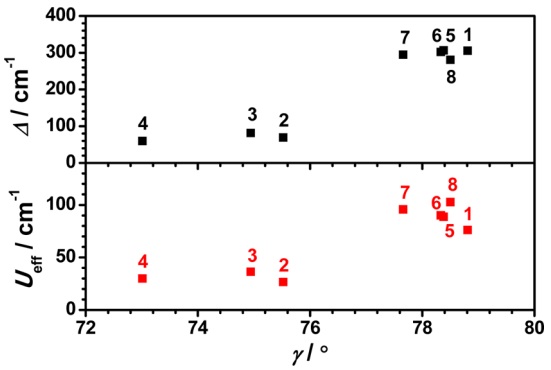

Figure 10. Δ vs γ plots and U_{eff} vs γ plot for compounds **1**–**8**.

energy barrier. In this family of SIMs, the remote substituent and countercation can regulate the coordination symmetry of central Co(II) ion, and therefore tune the anisotropy energy barrrier significantly. Our study demonstrates that the angular parameters and CShMs calculation of molecular structure can predict the magnetic anisotropy in this family compounds, which will also guide us to design new SIMs with similar symmetry in the future.

Circular Dichroism (CD) Spectrum Studies. To investigate the chiral behavior of this type of $Co^{II}Co^{III}_3$ cluster, the optical activity and enantiomeric nature of compounds **2R** and **2S** were confirmed by circular dichroism (CD) spectra as an example in both solution and the solid state. In DMF solution, the spectrum of **2R** exhibits a positive Cotton effect at λ_{max} = 286, and 405 nm and the negative signal at λ_{max} = 326, 458, and 686 nm, while **2S** shows Cotton effects of the opposite sign at the same wavelengths. It is notable the signals of complexes are very strong, compared to that of ligands. The CD signals of the two complexes form a mirror symmetry image very well, and they also indicate that they are enantiomeric compounds (see Figure 11). The solid-state CD

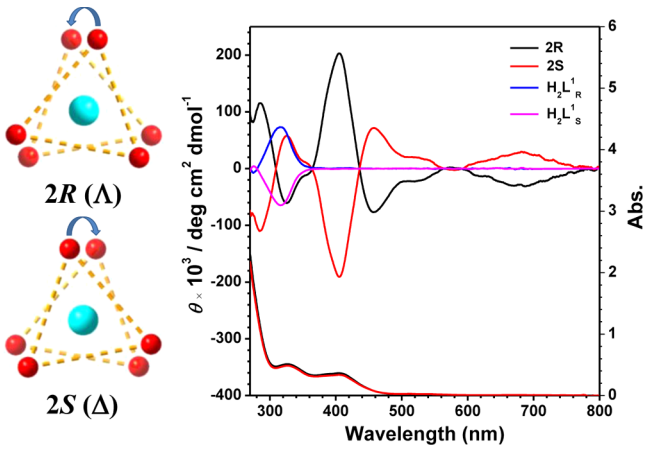

Figure 11. CD spectra of **2R**, **2S**, $H_2L^1_R$, and $H_2L^1_S$ and UV-vis spectrum of **2R** and **2S** at 298 K (5×10^{-5} M, DMF).

spectra gives almost the same signals compared to those in solution, which revealed the optical activity in solution and solid state is consistent (see Figure S74 in the Supporting Information). The CD intensity is much larger, compared to that of ligand with the same concentration. According to the crystal structure, the chirality of the whole compound mainly comes from the $Co^{II}Co^{III}_3O_6$ propeller. The absolute direction

DOI: 10.1021/acs.inorgchem.5b00526
Inorg. Chem. 2015, 54, 5475–5486

of propeller is induced by the chiral ligand. The absolute propeller configurations of central Co(II) sphere of **2R** and **2S** are Λ and Δ, respectively. However, the absolute configuration of three peripheral Co(III) spheres of **2R** and **2S** are Δ and Λ, respectively. The absolute configurations of central Co(II) ion and peripheral Co(III) ion are opposite. These results also demonstrate that the chirality has successfully transferred from the ligand to the coordination sphere of metal ions in the cluster.

CONCLUSIONS

In summary, a new family of air-stable tetranuclear $Co^{II}Co^{III}_3$ clusters with different chiral Schiff-based ligand derivatives were synthesized and magnetically characterized. All compounds behave as a 3d transition-metal single-molecule magnet (SMM) and possess considerable anisotropic energy barriers. The SMM behavior of this family compounds originates from the central sole paramagnetic Co(II) ion in approximate D_3 symmetry. Interestingly, the anisotropy energy barrier can be increased significantly from 38 K to 147 K by the remote substituent of the Schiff-base ligand and the countercation through regulating the coordination symmetry of central Co(II) ion. According to theoretical calculations and magnetostructural correlation studies, the coordination symmetry of central Co(II) ion is a key factor to affect the anisotropy energy barrier. Although the reports of field-induced slow magnetic relaxation from mononuclear 3d transition complexes continuously emerge, the examples of slow relaxation in the absence of dc field are still limited. This work will not enrich the family of 3d transition-metal single-ion magnets (SIMs), but it will guide us to discover new SIMs with similar local coordination symmetry. Further comprehensive theoretical research on this family SIMs is underway and will be reported in the near future.

ASSOCIATED CONTENT

Supporting Information

Listings of structural data, magnetic characterization, and circular dichroism (Figures S1−S73, Tables S1−S17), and a cif file of eight complexes (**2R**, **2S**, **3R**−**8R**). The Supporting Information is available free of charge on the ACS Publications website at DOI: 10.1021/acs.inorgchem.5b00526.

AUTHOR INFORMATION

Corresponding Authors

*E-mail: yyzhu@hfut.edu.cn (Y. Y. Zhu).
*E-mail: gaosong@pku.edu.cn (S. Gao).

Author Contributions

The manuscript was written through the contributions of all of the authors.

Funding

This work was supported by NSFC (Nos. 21290171, 21321001, 21302035, and 21371043), the National Basic Research Program (No. 2013CB933401), the Priority Academic Program Development of Jiangsu Higher Education Institutions, and the Fundamental Research Funds for the Central Universities.

Notes

The authors declare no competing financial interest.

ACKNOWLEDGMENTS

We thank Dr. X. Hao and Dr. T.-L. Liang (ICCAS), and Dr. Z.-Q. Gao and Dr. G.-C. Chang (Beijing Synchrotron Radiation Facility, Institute of High Energy Physics, Chinese Academy of Sciences) for the help of X-ray measurement, Prof. C.-M. Liu (ICCAS) for help of magnetic measurement, and Prof. Z.-W. Ouyang (Wuhan National High Magnetic Field Center) for help of high magnetic field measurement. We also thank Prof. J. van Slageren (Uniiversität Stuttgart), Prof. H. Zhang (Xiamen University), and Dr. S.-D. Jiang (LNCMI-CNRS) for helpful discussion.

REFERENCES

(1) (a) Gatteschi, D.; Sessoli, R.; Villain, J. *Molecular Nanomagnets*; Oxford University Press: Oxford, U.K., 2006. (b) Sessoli, R.; Gatteschi, D. *Angew. Chem., Int. Ed.* **2003**, *42*, 268−297.

(2) (a) Sessoli, R.; Tsai, H.-L.; Schake, A. R.; Wang, S.-Y.; Vincent, J. B.; Folting, K.; Gatteschi, D.; Christou, G.; Hendrichson, D. N. *J. Am. Chem. Soc.* **1993**, *115*, 1804−1816. (b) Sessoli, R.; Gatteschi, D.; Caneschi, A.; Novak, M. A. *Nature* **1993**, *365*, 141−143.

(3) (a) Aromí, G.; Brechin, B. *Struct. Bonding (Berlin)* **2006**, *122*, 1−69. (b) Sessoli, R.; Powell, A. K. *Coord. Chem. Rev.* **2009**, *253*, 2328−2341. (c) Sorace, L.; Benelli, C.; Gattechi, D. *Chem. Soc. Rev.* **2011**, *40*, 3092−3104. (c) Zhang, P.; Guo, Y.-N.; Tang, J. *Coord. Chem. Rev.* **2013**, *257*, 1728−1763.

(4) (a) Wernsdeorfer, W.; Sessoli, R. *Science* **1999**, *284*, 133−135. (b) Leuenberger, M. N.; Loss, D. *Nature* **2001**, *410*, 789−793. (c) Bogani, L.; Wernsdorfer, W. *Nat. Mater.* **2008**, *7*, 179−186. (d) Henderson, J. J.; Koo, C.; Feng, P. L.; del Barco, E.; Hill, S.; Tupitsyn, I. S.; Stamp, P. C. E.; Hendrickson, D. N. *Phys. Rev. Lett.* **2009**, *103*, 017202.

(5) (a) Milios, C. J.; Vinslava, A.; Wernsdorfer, W.; Moggach, S.; Parsons, S.; Perlepes, S. P.; Christou, G.; Brechin, E. K. *J. Am. Chem. Soc.* **2007**, *129*, 2754−2755. (b) Yoshihara, D.; Karasawa, S.; Koga, N. *J. Am. Chem. Soc.* **2008**, *130*, 10460−10461.

(6) (a) Ishikawa, N.; Sugita, M.; Ishikawa, T.; Koshihara, S.; Kaizu, Y. *J. Am. Chem. Soc.* **2003**, *125*, 8694−8695. (b) Ishikawa, N.; Sugita, M.; Ishikawa, T.; Koshihara, S.; Kaizu, Y. *J. Phys. Chem. B* **2004**, *108*, 11265−11271.

(7) (a) AlDamen, M. A.; Clemente-Juan, J. M.; Coronado, E.; Marti-Gastaldo, C.; Gaita-Ariño, A. *J. Am. Chem. Soc.* **2008**, *130*, 8874−8875. (b) Rinehart, J. D.; Long, J. R. *J. Am. Chem. Soc.* **2009**, *131*, 12558−12559. (c) Rinehart, J. D.; Meihaus, K. R.; Long, J. R. *J. Am. Chem. Soc.* **2010**, *132*, 7572−7573. (d) Jiang, S.-D.; Wang, B.-W.; Su, G.; Wang, Z.-M.; Gao, S. *Angew. Chem., Int. Ed.* **2010**, *49*, 7448−7451. (e) Li, D.-P.; Wang, T.-W.; Li, C.-H.; Liu, D.-S.; Li, Y.-Z.; You, X.-Z. *Chem. Commun.* **2010**, *46*, 2929−2931. (f) Bi, Y.; Guo, Y.-N.; Zhao, L.; Guo, Y.; Lin, S.-Y.; Jiang, S.-D.; Tang, J.-K.; Wang, B.-W.; Gao, S. *Chem.−Eur. J.* **2011**, *17*, 12476−12481. (g) Jiang, S.-D.; Wang, B.-W.; Sun, H.-L.; Wang, Z.-M.; Gao, S. *J. Am. Chem. Soc.* **2011**, *133*, 4730−4733. (h) Magnani, N.; Apostolidis, C.; Morgenstern, A.; Colineau, E.; Griveau, J.-C.; Bolvin, H.; Walter, O.; Caciuffo, R. *Angew. Chem., Int. Ed.* **2011**, *50*, 1696−1698. (i) Cucinotta, G.; Perfetti, M.; Luzon, J.; Etienne, M.; Car, P.-E.; Caneschi, A.; Calvez, G.; Bernot, K.; Sessoli, R. *Angew. Chem., Int. Ed.* **2012**, *51*, 1606−1610. (j) Liu, J.-L.; Yuan, K.; Leng, J.-D.; Ungur, L.; Wernsdorfer, W.; Guo, F.-S.; Chibotaru, L. F.; Tong, M.-L. *Inorg. Chem.* **2012**, *51*, 8538. (k) Liu, J.-L.; Chen, Y.-C.; Zheng, Y.-Z.; Lin, W.-Q.; Ungur, L.; Wernsdorfer, W.; Chibotaru, L. F.; Tong, M.-L. *Chem. Sci.* **2013**, *4*, 3310−3316. (l) Guo, Y.-N.; Ungur, L.; Granroth, G. E.; Powell, A. K.; Wu, C.; Nagler, S. E.; Tang, J.; Chibotaru, L. F.; Cui, D. *Sci. Rep.* **2014**, *4*, 5471. (m) Zhang, P.; Zhang, L.; Wang, C.; Xue, S.; Lin, S.-Y.; Tang, J. *J. Am. Chem. Soc.* **2014**, *136*, 4484−4487.

(8) (a) Liu, Q.-D.; Li, J.-R.; Gao, S.; Ma, B.-Q.; Zhou, Q.-Z.; Yu, K.-B.; Liu, H. *Chem. Commun.* **2000**, 1685−1686. (b) Gao, S.; Ma, B.-Q.; Sun, H.-L.; Su, G. *Abstract ICMM* **2002**, pA-63. (c) Zhang, Y.-Z. Ph.D. Thesis, Peking University, Beijing, 2005.

(9) (a) Jurca, T.; Farghal, A.; Lin, P.-H.; Korobkov, I.; Murugesu, M.; Richeson, D. S. *J. Am. Chem. Soc.* **2011**, *133*, 15814−15817. (b) Vallejo, J.; Castro, I.; Ruiz-García, R.; Cano, J.; Julve, M.; Lloret, F.; Munno, G. D.; Wernsdorfer, W.; Pardo, E. *J. Am. Chem. Soc.* **2012**, *134*, 15704−

DOI: 10.1021/acs.inorgchem.5b00526
Inorg. Chem. 2015, 54, 5475−5486

15707. (c) Zadrozny, J. M.; Liu, J.; Piro, N. A.; Chang, C. J.; Hill, S.; Long, J. R. *Chem. Commun.* **2012**, *48*, 3927−3929. (d) Colacio, E.; Ruiz, J.; Ruiz, E.; Cremades, E.; Krzystek, J.; Carretta, S.; Cano, J.; Guidi, T.; Wernsdorfer, W.; Brechin, E. K. *Angew. Chem., Int. Ed.* **2013**, *52*, 9130−9134. (e) Habib, F.; Luca, O. R.; Vieru, V.; Shiddiq, M.; Korobkov, I.; Gorelsky, S. I.; Takase, M. K.; Chibotaru, L. F.; Hill, S.; Crabtree, R. H.; Murugesu, M. *Angew. Chem., Int. Ed.* **2013**, *52*, 11290−11293. (f) Yang, F.; Zhou, Q.; Zhang, Y.-Q.; Zeng, G.; Li, G.-H.; Shi, Z.; Wang, B.-W.; Feng, S.-H. *Chem. Commun.* **2013**, *49*, 5289−5291. (g) Cao, D.-K.; Feng, J.-Q.; Ren, M.; Gu, Y.-W.; Song, Y.; Ward, M. D. *Chem. Commun.* **2013**, *49*, 8863−8865. (h) Wu, D.-Y.; Zhang, X.-X.; Huang, P.; Huang, W.; Ruan, M.-Y.; Ouyang, Z. W. *Inorg. Chem.* **2013**, *52*, 10976−10982. (i) Huang, W.; Liu, T.; Wu, D.-Y.; Cheng, J.-J.; Ouyang, Z. W.; Duan, C.-Y. *Dalton Trans.* **2013**, *42*, 15326−15331. (j) Eichhöfer, A.; Lan, Y.; Mereacre, V.; Bodenstein, T.; Weigend, F. *Inorg. Chem.* **2014**, *53*, 1962−1974. (k) Boča, R.; Miklovič, J.; Titiš, J. *Inorg. Chem.* **2014**, *53*, 2367−2369. (l) Herchel, R.; Váhovská, L.; Potočňák, I.; Trávníček, Z. *Inorg. Chem.* **2014**, *53*, 5896−5898. (m) Gómez-Coca, S.; Urtizberea, A.; Cremades, E.; Alonso, P. J.; Camón, A.; Ruiz, E.; Luis, F. *Nat. Commun.* **2014**, *5*, 4300. (n) Chen, L.; Wang, J.; Wei, J.-M.; Wernsdorfer, W.; Chen, X.-T.; Zhang, Y.-Q.; Song, Y.; Xue, Z.-L. *J. Am. Chem. Soc.* **2014**, *136*, 12213−12216. (o) Saber, M. R.; Dunbar, K. R. *Chem. Commun.* **2014**, *50*, 12266−12269. (p) Nedelko, N.; Kornowicz, A.; Justyniak, I.; Aleshkevych, P.; Prochowicz, D.; Krupiński, P.; Dorosh, O.; Ślawska-Waniewska, A.; Lewiński, J. *Inorg. Chem.* **2014**, *53*, 12870−12876. (q) Huang, X.-C.; Zhou, C.; Shao, D.; Wang, X.-Y. *Inorg. Chem.* **2014**, *53*, 12671−12673. (r) Ruamps, R.; Luke, J.; Batchelor, L. J.; Guillot, R.; Zakhia, G.; Barra, A.-L.; Wernsdorfer, W.; Guihéry, N.; Mallah, T. *Chem. Sci.* **2014**, 3418−3424. (s) Zhu, Y.-Y.; Yin, T.-T.; Liu, C.-W.; Gao, C.; Wu, Z.-Q.; Zhang, Y.-Q.; Wang, B.-W.; Gao, S. *Supramol. Chem.* **2015**, *27*, 401−406. (t) Ion, A. E.; Nica, S.; Madalan, A. M.; Shova, S.; Vallejo, J.; Julve, M.; Lloret, F.; Andruh, M. *Inorg. Chem.* **2015**, *54*, 16−18. (u) Schweinfurth, D.; Sommer, M. G.; Atanasov, M.; Demeshko, S.; Hohloch, S.; Meyer, F.; Neese, F.; Sarkar, B. *J. Am. Chem. Soc.* **2015**, *137*, 1993−2005. (v) Zhu, Y.-Y.; Zhu, M.-S.; Yin, T.-T.; Meng, Y.-S.; Wu, Z.-Q.; Zhang, Y.-Q.; Gao, S. *Inorg. Chem.* **2015**, *54*, 3716−3718. (w) Zhang, Y.-Z.; Brown, A. J.; Meng, Y.-S.; Sun, H.-L.; Gao, S. *Dalton Trans.* **2015**, *44*, 2865−2870.

(10) (a) Zadrozny, J. M.; Long, J. R. *J. Am. Chem. Soc.* **2011**, *133*, 20732−20734. (b) Zadrozny, J. M.; Telser, J.; Long, J. R. *Polyhedron* **2013**, *64*, 209−217. (c) Zhu, Y.-Y.; Cui, C.; Zhang, Y.-Q.; Jia, J.-H.; Guo, X.; Gao, C.; Qian, K.; Jiang, S.-D.; Wang, B.-W.; Wang, Z.-M.; Gao, S. *Chem. Sci.* **2013**, *4*, 1802−1806. (d) Gomez-Coca, S.; Cremades, E.; Aliaga-Alcalde, N.; Ruiz, E. *J. Am. Chem. Soc.* **2013**, *135*, 7010−7018. (e) Fataftah, M. S.; Zadrozny, J. M.; Rogers, D. M.; Freedman, D. E. *Inorg. Chem.* **2014**, *53*, 10716−10721.

(11) Zadrozny, J. M.; Xiao, D. J.; Atanasov, M.; Long, G. J.; Grandjean, F.; Neese, F.; Long, J. R. *Nat. Chem.* **2013**, *5*, 577−581.

(12) (a) Freedman, D. E.; Harman, W. H.; Harris, T. D.; Long, G. J.; Chang, C. J.; Long, J. R. *J. Am. Chem. Soc.* **2010**, *132*, 1224−1225. (b) Harman, W. H.; Harris, T. D.; Freedman, D. E.; Fong, H.; Chang, A.; Rinehart, J. D.; Ozarowski, A.; Sougrati, M. T.; Grandjean, F.; Long, G. J.; Long, J. R.; Chang, C. J. *J. Am. Chem. Soc.* **2010**, *132*, 18115−18126. (c) Lin, P.-H.; Smythe, N. C.; Gorelsky, S. I.; Maguire, S.; Henson, N. J.; Korobkov, I.; Scott, B. L.; Gordon, J. C.; Baker, R. T.; Murugesu, M. *J. Am. Chem. Soc.* **2011**, *133*, 15806−15809. (d) Weismann, D.; Sun, Y.; Lan, Y.; Wolmershäuser, G.; Powell, A. K.; Sitzmann, H. *Chem.−Eur. J.* **2011**, *17*, 4700−4704. (e) Zadrozny, J. M.; Atanasov, M.; Bryan, A. M.; Lin, C.-Y.; Rekken, B. D.; Power, P. P.; Neese, F.; Long, J. R. *Chem. Sci.* **2013**, *4*, 125−138. (f) Atanasov, M.; Zadrozny, J. M.; Long, J. R.; Neese, F. *Chem. Sci.* **2013**, *4*, 139−156. (g) Feng, X.; Mathonière, C.; Jeon, I.-R.; Rouzières, M.; Ozarowski, A.; Aubrey, M. L.; Gonzalez, M. I.; Clérac, R.; Long, J. R. *J. Am. Chem. Soc.* **2013**, *135*, 15880−15884. (h) Mathonière, C.; Lin, H.-J.; Siretanu, D.; Clèrac, R.; Smith, J. M. *J. Am. Chem. Soc.* **2013**, *135*, 19083−19086.

(13) Mossin, S.; Tran, B. L.; Adhikari, D.; Pink, M.; Heinemann, F. W.; Sutter, J.; Szilagyi, R. K.; Meyer, K.; Mindiola, D. J. *J. Am. Chem. Soc.* **2012**, *134*, 13651−13661.

(14) Poulten, R. C.; Page, M. J.; Algarra, A. G.; Le Roy, J. J.; López, I.; Carter, E.; Llobet, A.; Macgregor, S. A.; Mahon, M. F.; Murphy, D. M.; Murugesu, M.; Whittlesey, M. K. *J. Am. Chem. Soc.* **2013**, *135*, 13640−13643.

(15) (a) Ishikawa, R.; Miyamoto, R.; Nojiri, H.; Breedlove, B. K.; Yamashita, M. *Inorg. Chem.* **2013**, *52*, 8300−8302. (b) Grigoropoulos, A.; Pissas, M.; Papatolis, P.; Psycharis, V.; Kyritsis, P.; Sanakis, Y. *Inorg. Chem.* **2013**, *52*, 12869−12871. (c) Vallejo, J.; Pascual-Alvarez, A.; Cano, J.; Castro, I.; Julve, M.; Lloret, F.; Krzystek, J.; De Munno, G.; Armentano, D.; Wernsdorfer, W.; Ruiz-Garcia, R.; Pardo, E. *Angew. Chem., Int. Ed.* **2013**, *52*, 14075−14079. (d) Craig, G. A.; Marbey, J. J.; Hill, S.; Roubeau, O.; Parsons, S.; Murrie, M. *Inorg. Chem.* **2015**, *54*, 13−15.

(16) (a) Martnez-Lillo, J.; Mastropietro, T. F.; Lhotel, E.; Paulsen, C.; Cano, J.; De Munno, G.; Faus, J.; Lloret, F.; Julve, M.; Nellutla, S.; Krzystek, J. *J. Am. Chem. Soc.* **2013**, *135*, 13737−13748. (b) Pedersen, K. S.; Sigrist, M.; Sørensen, M. A.; Barra, A.-L.; Weyhermüller, T.; Piligkos, S.; Thuesen, C. A.; Vinum, M. G.; Mutka, H.; Weihe, H.; Clérac, R.; Bendix, J. *Angew. Chem., Int., Ed.* **2014**, *53*, 1351−1354.

(17) Sheldrick, G. M. *SHELXS-97*; University of Göttingen, Göttingen, Germany, 1990.

(18) Sheldrick, G. M. *SHELXS-97*; University of Göttingen, Göttingen, Germany, 1990.

(19) Spek, A. L. *PLATON, A Multipurpose Crystallographic Tool*; Utrecht University: Utrecht, The Netherlands, 2002.

(20) Carlin, R. L. *Magnetochemistry*; Springer−Verlag Press: Berlin, Heidelberg, 1986.

(21) (a) Zhu, Y.-Y.; Guo, X.; Cui, C.; Wang, B.-W.; Wang, Z.-M.; Gao, S. *Chem. Commun.* **2011**, *47*, 8049−8051. (b) Zhu, Y.-Y.; Cui, C.; Qian, K.; Yin, J.; Wang, B.-W.; Wang, Z.-M.; Gao, S. *Dalton Trans.* **2014**, *43*, 11897−11907. (c) Zhu, Y.-Y.; Yin, T.-T.; Jiang, S.-D.; Barra, A.-L.; Wernsdorfer, W.; Neugebauer, P.; Marx, R.; Dörfel, M.; Wang, B.-W.; Wu, Z.-Q.; van Slageren, J.; Gao, S. *Chem. Commun.* **2014**, *50*, 15090−15093.

(22) Yin, J.; Yin, T.-T.; Gao, C.; Wang, B.-W.; Zhu, Y.-Y.; Wu, Z.-Q.; Gao, S. *Eur. J. Inorg. Chem.* **2014**, 5385−5390.

(23) Gregoli, L.; Danieli, C.; Barra, A.-L.; Neugebauer, P.; Pellegrino, G.; Poneti, G.; Sessoli, R.; Cornia, A. *Chem.−Eur. J.* **2009**, *15*, 6456−6467.

(24) (a) Pinsky, M.; Avnir, D. *Inorg. Chem.* **1998**, *37*, 5575−5582. (b) Alvarez, S.; Avnir, D.; Llunell, M.; Pinsky, M. *New J. Chem.* **2002**, *26*, 996−1009. (c) Alvarez, S.; Alemany, P.; Casanova, D.; Cirera, J.; Llunell, M.; Avnir, D. *Coord. Chem. Rev.* **2005**, *249*, 1693−1708.

(25) Llunell, M.; Casanova, D.; Cirera, J.; Alemany, P.; Alvarez, S. *SHAPE*, version 2.0; Universitat de Barcelona, Barcelona, Spain, 2010.

(26) Cole, K. S.; Cole, R. H. *J. Chem. Phys.* **1941**, *9*, 341−351.

(27) Karlström, G.; Lindh, R.; Malmqvist, P.-Å.; Roos, B. O.; Ryde, U.; Veryazov, V.; Widmark, P.-O.; Cossi, M.; Schimmelpfennig, B.; Neogrady, P.; Seijo, L. *Comput. Mater. Sci.* **2003**, *28*, 222−239.

(28) Seijo, L.; Barandiarán, Z. *Computational Chemistry: Reviews of Current Trends*, Vol. *4*; World Scientific: Singapore, 1999; pp 55−152.

(29) Chilton, N. F.; Anderson, R. P.; Turner, L. D.; Soncini, A.; Murray, K. S. *J. Comput. Chem.* **2013**, *34*, 1164−1175.

(30) Wei, J.-M.; Zhang, Y.-Q. *Inorg. Chem.* **2015**, *54*, 1203−1205.

DOI: 10.1021/acs.inorgchem.5b00526
Inorg. Chem. 2015, 54, 5475−5486